

Planar structure of organic photodetector for low dark current

Mohammad Nofil, Amirul Ashraf Md Sabri, Fadlan Arif Natashah, Tahani M Bawazeer, Mohammad S Alsoufi, Nur Adilah Roslan, and Azzuliani Supangat

Citation : Chin. Phys. B, 2025, 34 (**2**): 024204. DOI: 10.1088/1674-1056/ad9731
Journal homepage: http://cpb.iphy.ac.cn; http://iopscience.iop.org/cpb

What follows is a list of articles you may be interested in

A broadband self-powered UV photodetector of a β-Ga_2O_3/γ-CuI p-n junction

Wei-Ming Sun(孙伟铭), Bing-Yang Sun(孙兵阳), Shan Li(李山), Guo-Liang Ma(麻国梁), Ang Gao(高昂), Wei-Yu Jiang(江为宇), Mao-Lin Zhang(张茂林), Pei-Gang Li(李培刚), Zeng Liu(刘增), and Wei-Hua Tang(唐为华)
Chin. Phys. B, 2022, 31 (**2**): 024205. DOI: 10.1088/1674-1056/ac29b3

Total ionizing dose effects in pinned photodiode complementary metal-oxide-semiconductor transistor active pixel sensor

Lin-Dong Ma(马林东), Yu-Dong Li(李豫东), Lin Wen(文林), Jie Feng(冯婕), Xiang Zhang(张翔), Tian-Hui Wang(王田珲), Yu-Long Cai(蔡毓龙), Zhi-Ming Wang(王志铭), Qi Guo(郭旗)
Chin. Phys. B, 2018, 27 (**10**): 104207. DOI: 10.1088/1674-1056/27/10/104207

Error analysis and Stokes parameter measurement of rotating quarter-wave plate polarimeter

Dan-Dan Zhi(支丹丹), Jian-Jun Li(李健军), Dong-Yang Gao(高冬阳), Wen-Chao Zhai(翟文超), Xiong-Hao Huang(黄雄豪), Xiao-Bing Zheng(郑小兵)
Chin. Phys. B, 2017, 26 (**12**): 124201. DOI: 10.1088/1674-1056/26/12/124201

Analysis of proton and γ-ray radiation effects on CMOS active pixel sensors

Lindong Ma(马林东), Yudong Li(李豫东), Qi Guo(郭旗), Lin Wen(文林), Dong Zhou(周东), Jie Feng(冯婕), Yuan Liu(刘元), Junzhe Zeng(曾骏哲), Xiang Zhang(张翔), Tianhui Wang(王田珲)
Chin. Phys. B, 2017, 26 (**11**): 114212. DOI: 10.1088/1674-1056/26/11/114212

Asymmetrical plasmon reflections in tapered graphene ribbons with wrinkle edges

Cui Yang(杨翠), Runkun Chen(陈闰堃), Yuping Jia(贾玉萍), Liwei Guo(郭丽伟), Jianing Chen(陈佳宁)
Chin. Phys. B, 2017, 26 (**7**): 074220. DOI: 10.1088/1674-1056/26/7/074220

Planar structure of organic photodetector for low dark current

Mohammad Nofil[1], Amirul Ashraf Md Sabri[1], Fadlan Arif Natashah[1], Tahani M Bawazeer[2], Mohammad S Alsoufi[3], Nur Adilah Roslan[4,†], and Azzuliani Supangat[1,‡]

[1] *Low Dimensional Materials Research Centre, Department of Physics, Faculty of Science, Universiti Malaya, Kuala Lumpur,* 50603, *Malaysia*
[2] *Department of Chemistry, Faculty of Applied Science, Umm Al-Qura University, Makkah, Saudi Arabia*
[3] *Mechanical Engineering Department, College of Engineering and Islamic Architecture, Umm Al-Qura University, Makkah, Saudi Arabia*
[4] *Department of Physics, Faculty of Science, Universiti Putra Malaysia, Serdang,* 43400, *Malaysia*

(Received 2 July 2024; revised manuscript received 22 November 2024; accepted manuscript online 26 November 2024)

The focus of this study is on investigating the vanadyl 2,9,16,23-tetraphenoxy-29H, 31H-phthalocyanine (VOPcPhO) and its blend with o-xylenyl C60 bis-adduct (OXCBA), for use as a lateral ultraviolet organic photodetector. The research focuses on improving dark current reduction, which is a challenge in lateral organic photodetector. By integrating the OXCBA, low dark current values of 4.83 $\mathrm{nA\cdot cm^{-2}}$ ($D^*_{\mathrm{shot}} = 1.414 \times 10^{11}$ Jones) have been achieved as compared to the stand-alone VoPcPhO device of 14.06 $\mathrm{nA\cdot cm^{-2}}$. The major contributing factors to dark current reduction are due to the efficient charge transfer at the photoactive-electrode interface, the deep highest occupied molecular orbital (HOMO) level of OXCBA, which leads to favorable energy level alignments hindering hole injection, and the occurrence of bulk heterojunction vertical phase segregation between VOPcPhO and OXCBA. These findings shed light on the relationship between the organic photoconductor's material composition, morphology, and performance metrics and open new avenues for metal phthalocyanine-based lateral ultraviolet organic photodetectors with low dark current and enhanced performance.

Keywords: small molecule, dark current, ultra-violet (UV) sensor, device physics

PACS: 42.79.Pw, 42.70.Jk, 61.82.Fk, 07.57.Kp

DOI: 10.1088/1674-1056/ad9731 **CSTR:** 32038.14.CPB.ad9731

1. Introduction

The optoelectronic industry has rapidly revolutionized in recent years, leading to numerous technological advancements ranging from displays and sensors to solar cells and communication. The photodetector is a key player in this progress, converting light particles into electrical signals. Photodetectors are widely used in modern electronics like displays, phones, solar cells, medical imaging, and sensing.[1–3] While prevalent photodetectors rely on expensive inorganic semiconductors like silicon and gallium phosphide for superior performance,[4–6] their production costs and inflexibility limit their scalability and compatibility with flexible electronics.

Organic photodetectors (OPDs) based on organic semiconductors such as polymers and small molecules have emerged as a promising alternative to their inorganic counterparts over the last decade due to their inherent advantages, ease of processing, lower production costs, flexibility, and scalability.[7,8] Metal phthalocyanines (MPcs) are a specific class of organic semiconducting compounds with a central metal atom or ion coordinated with an aromatic, macrocyclic compound called *phthalocyanine*, which has gained significant interest due to their desirable optical, chemical, thermal, and electrical stability. However, most MPc-based devices have focused on the visible-NIR region of the electromagnetic spectrum with a bit of emphasis on the ultraviolet-sensitive OPDs.

Vanadyl 2,9,16,23-tetra phenoxy-29H, 31H-phthalocyanine (VOPcPhO) is a metal phthalocyanine with a vanadyl (VO) group as the central metal ion along with a phosphine oxide (PhO) derivative. VOPcPhO exhibits a broad absorption spectrum ranging from ultra-violet (UV) to far-visible/NIR regions. Due to this characteristic, it has been rendered a promising candidate for OPD applications in various works of literature.[9,10] Given VOPcPhO's pronounced UV-absorption capabilities, this research specifically focuses on developing a VOPcPhO-based lateral organic photodetector designed for UV detection.

In general, MPcs-based photodetectors can be classified as photoconductors, photodiodes and phototransistors. A photoconductor is the simplest type of three-device structure that utilize the photoconductive effect in two-terminal devices. An interest in utilizing a lateral OPD arrangement has evolved, where two contacts are placed on opposite sides of the photoactive layer with a small gap between them.[11] Applying an external bias across the electrodes establishes an electrical "path" across the gap, allowing the collection of photogenerated carriers when the semiconductor is exposed to light.

†Corresponding author. E-mail: azzuliani@um.edu.my
‡Corresponding author. E-mail: nur.adilah@upm.edu.my

© 2025 Chinese Physical Society and IOP Publishing Ltd. All rights, including for text and data mining, AI training, and similar technologies, are reserved.

This means the electrodes are not in the light path of the signal, and therefore, they do not need to be transparent.

However, lateral OPDs generally suffer from high dark/leakage current values. Several strategies have been employed to reduce the dark current in OPDs. One of the most promising methods to reduce charge injection is to create a significant energy level offset between the Fermi level or the work function of the electrode and the HOMO–LUMO (highest occupied molecular orbital–lowest unoccupied molecular orbital) offset level of the donor-acceptor molecule at the electrode:photoactive interface.[12] A deeper HOMO–LUMO offset can facilitate more effective charge separation at the donor–acceptor interface due to a stronger electron and hole transfer driving force. On top of that, the reduction of charge injection helps control the accumulation of space charges near the edges of the metallic contact, which, in turn, minimizes the facilitation of charge carrier movement in the absence of light and reduces the dark current in the device.[13]

Several studies have focused on using donor molecules with deep-lying HOMO levels, resulting in dark currents as low as 10^{-7} mA $\cdot$ cm^{-2}.[14] Recently, solution-processed bulk heterojunction (BHJ) photoactive layers have been explored to determine their effect on reducing the dark current due to vertical phase segregation.[15] Low dark current values of 1.6×10^{-7} A $\cdot$ cm^{-2} and 3.4×10^{-10} A $\cdot$ cm^{-2} for P3HT/PC$_{71}$BM[16] and Lisicon PV-D4650:PCBM[17] sequentially deposited bulk heterojunction (BHJ) active layers, respectively, have been reported in the past. However, most of the progress in reducing dark current has been made on vertical structures of OPDs with little emphasis on the much simpler planar/lateral structure.

Taking these factors into consideration, we aim to optimize the performance of the UV-sensitive photodetector by doping VOPcPhO-acceptor material with a fullerene donor derivative having a deep HOMO level, namely, o-xylenyl C60 bis-adduct (OXCBA) to form a solution-processed BHJ photoactive layer. The OXCBA has gained considerable attention recently due to its comparable properties with PCBM.[18,19] In this study, we fabricate a novel MPc-based UV-sensitive photodetector and explore the compatibility of OXCBA with VOPcPhO from the morphological, optical, and electrical aspects with a focus on reducing the dark current density in the fabricated UV-photodetector.

2. Experimental details

The molecular structure of the VOPcPhO (p-type) and the OXCBA (n-type) is shown in Fig. 1(a). Both materials were purchased from Sigma Aldrich Inc. and were used in an as-received state. Chloroform, a polar organic solvent, was used to separately dissolve both VOPcPhO and OXCBA with a concentration of 10 mg/mL each using a magnetic stirrer at 700 rpm for 24 hours. The dissolved VOPcPhO and OXCBA were mixed in a 1:1 molar ratio to prepare the PN solution. Simultaneously, 1.5 cm $\times$ 2.0 cm glass substrates were prepared and cleaned with detergent, distilled water, acetone, and isopropyl alcohol for 15 min each in an ultrasonic agitator. The glass substrates were then blow-dried using nitrogen.

The prepared solutions were then fabricated into thin films using the spin-coating method at 2000 rpm for 30 s to form a 150-nm thin layer. The deposited thin films were then subjected to thermal annealing at 80 °C for 15 min to improve the morphology of the layer. Later, a 100-nm aluminium layer was thermally deposited on the thin films using the physical vacuum deposition technique performed in a nitrogen glovebox under a base pressure of 2×10^{-7} bar (1 bar $= 10^5$ Pa). A minimal gap of 60 μm between the aluminium and the deposited thin film was made. The schematic mechanism of the fabricated devices and the energy level alignments are shown in Figs. 1(b) and 1(c), respectively. The devices were then stored in UV-cured epoxy and glass. The PN is defined as VOPcPhO:OXCBA film throughout the paper.

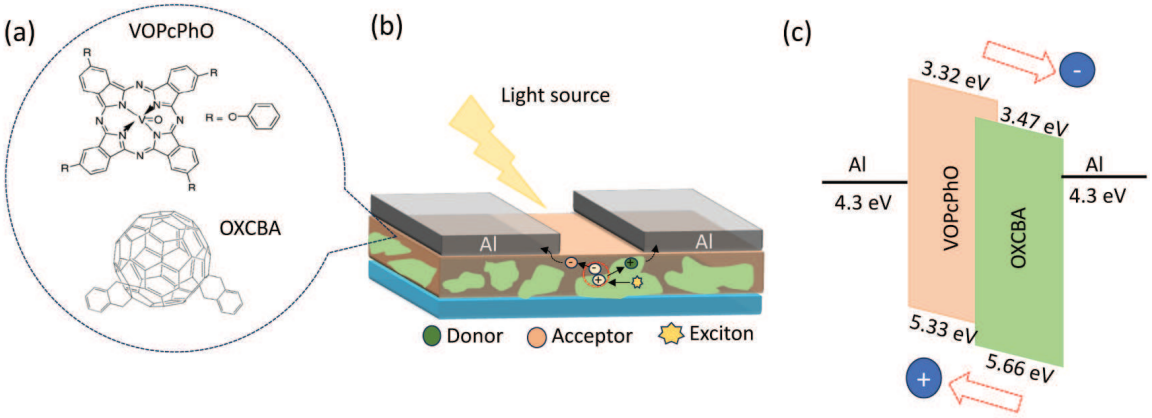


Fig. 1. (a) Molecular structure, (b) schematic illustration of the device structure, and (c) energy level diagram.[9,20]

The thin films were characterized using a UV-Vis spectrophotometer (Perkin LAMBDA 900, Waltham, MA, USA) under UV-visible-NIR irradiation to study their absorption spectra. The surface thickness of the films was determined using a surface profilometer (model Bruker Dektak XT, Billerica, MA, USA), while the morphology was characterized using an atomic force microscope (Hitachi AFM5100N using SI-DF3 cantilever). The electronic characterization of the fabricated devices was studied using the Kiethley 238 source measure unit and a UV light source of specific wavelength 365nm and an optical power density of 45 mW/cm^2.

3. Results and discussion

3.1. Blue shift absorption and rougher surface due to the addition of n-type

The UV-Vis spectroscopy was performed to determine the light absorption properties of the VOPcPhO and the effect of OXCBA on its absorption spectra. Figure 2(a) illustrates the absorption spectra of VOPcPhO. The most substantial absorption peak can be observed around the UV region at 344 nm, with a shoulder coming about at 395 nm. These peaks represent the Soret bands in the metal phthalocyanines.[21] Absorption peaks can also be observed at 715 nm, with a shoulder coming at 665 nm in the visible region of the spectrum. These peaks represent the Q-bands of metal phthalocyanine caused by strong first π–π^* in the phthalocyanine macrocycle, with the shoulder coming due to the exciton peak.[22,23]

The figure also illustrates the absorption spectra for the PN thin film. By adding the OXCBA, the absorbance in the UV region was increased dramatically, with the peak coming at 340 nm. This can be attributed to the absorption spectra of OXCBA, which demonstrates peak absorption in the UV region, specifically in the range of 300 nm–400 nm. It should also be noted that the absorption in the visible region dropped after adding OXCBA. This is again attributed to the fact that OXCBA has little to no absorption in the visible and NIR regions.

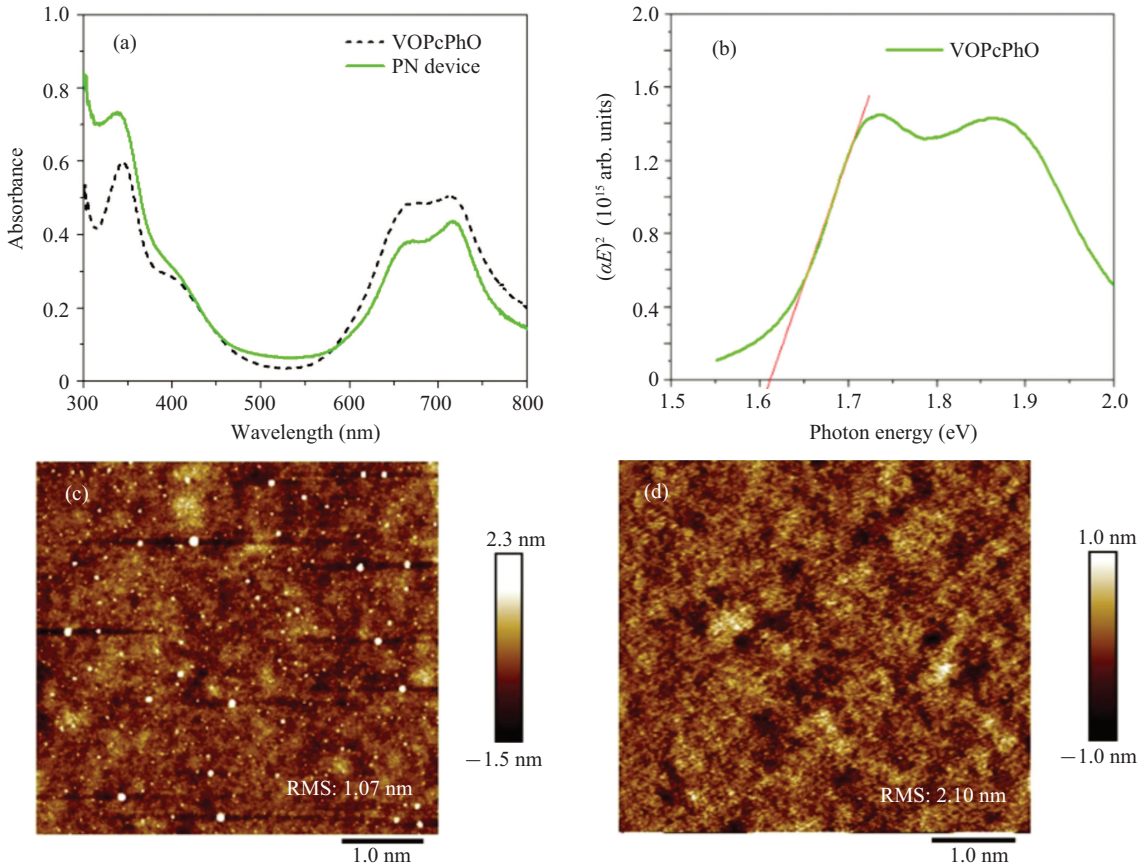


Fig. 2. (a) Absorption spectra of VOPcPhO and PN thin film and (b) Tauc plot for energy gap calculation and the AFM images of (c) VOPcPhO and (d) PN thin film.

Another important characteristic that can be determined from the absorption spectra is the energy gap, which can greatly impact the device's performance. The energy gap for VOPcPhO is determined using the Tauc plot method,[24] which makes use of the following equation:

$$(\alpha h\nu)^{1/n} = A^*(h\nu - E_g), \tag{1}$$

where h, ν, α, E_g, and A^* represent the Planck constant, photon frequency, absorption coefficient, energy gap, and slope

of the Tauc plot, respectively. The number of allowed direct ($n = 1/2$) or indirect ($n = 2$), and forbidden direct ($n = 3/2$) or indirect ($n = 3$) electronic transitions are determined by the value of n. A linear region from the plot of $(\alpha h\nu)^2$ against $(h\nu)$ is used to extrapolate the x-intercept to determine the value of E_g. The value of E_g for VOPcPhO was found to be 1.61 eV, which is in acceptance with values obtained in various literature.[25] The Tauc plot of VOPcPhO is shown in Fig. 2(b).

The surface morphology and roughness can also play a vital role in the charge transport properties of organic photodetectors.[26] To determine the surface roughness, the atomic force microscopy (AFM) technique was used, which relies on a cantilever to tap on the surface of the device. Figures 2(c) and 2(d) depicts the AFM images of the surface of both devices. The addition of OXCBA in a 1:1 ratio increased the surface roughness of the device from 1.07 nm to 2.10 nm. This indicates that OXCBA when added in a 1:1 ratio, deteriorates the surface and hence can harm the charge transport of the device and induce an electron–hole recombination.[27]

3.2. Reduced dark current by adding the OXCBA

Dark current in OPDs, often called leakage current, is caused by the charge injection carrier rate from the electrodes and can significantly impact the device's performance.[28,29] The HOMO and LUMO levels of the donor and acceptor materials, respectively, the charge injection barrier Φ_b, and the strength of the applied bias can play a crucial role in the charge injection dynamics of the OPDs. The electrode with a higher (lower) work function than the LUMO (HOMO) of the acceptor (donor) creates an energy level alignment that favors the injection of holes (electrons) from the higher (lower) work function electrode.

Figure 3(a) shows the J–V characteristics for both P and PN devices under dark conditions. The P device is defined as a stand-alone VOPcPhO device, while PN device is device is defined as VOPcPhO:OXCBA device. A decrease in the dark current density (J_d) from 14.06×10^{-9} A/cm^2 to 4.83×10^{-9} A/cm^2 is observed by the addition of OXCBA. This decrease in J_d can be attributed to the following reasons: the presence of an electron channel between the photoactive layer and the electrode interface[30] and the rate of charge injection carriers relies on the injection barrier Φ_b.[8] This barrier is determined by the difference between the acceptor's LUMO and the low work function electrode for electrons and the donor's HOMO and the high work function electrode for holes.[14] Since both the devices used in this experiment were fabricated to have the same aluminum electrodes, the injection barrier is determined solely by the HOMO and LUMO levels of the donor and acceptor, respectively. As a donor, OXCBA has a very deep HOMO level (5.66 eV),[31] which results in a high hole-injection barrier of 1.36 eV between the Al electrode and the photoactive layer thus blocking the hole injection from the electrodes caused by either thermal effects or impurities and lowering the J_d. The dark current characteristics of the OPD verify the vertical phase separation in the blend layer. The electrons injected from the cathode do not have to experience a high barrier of LUMO level and resulting in efficient injection as compared to stand-alone OPD. A similar process occurs for the holes at the anode.[32] This can lead to favorable energy level alignments at the photoactive: electrode interface, reducing charge injection from the electrodes, and enhancing the device's performance. These dark current reduction mechanisms are illustrated in Figs. 3(b) and 3(c).

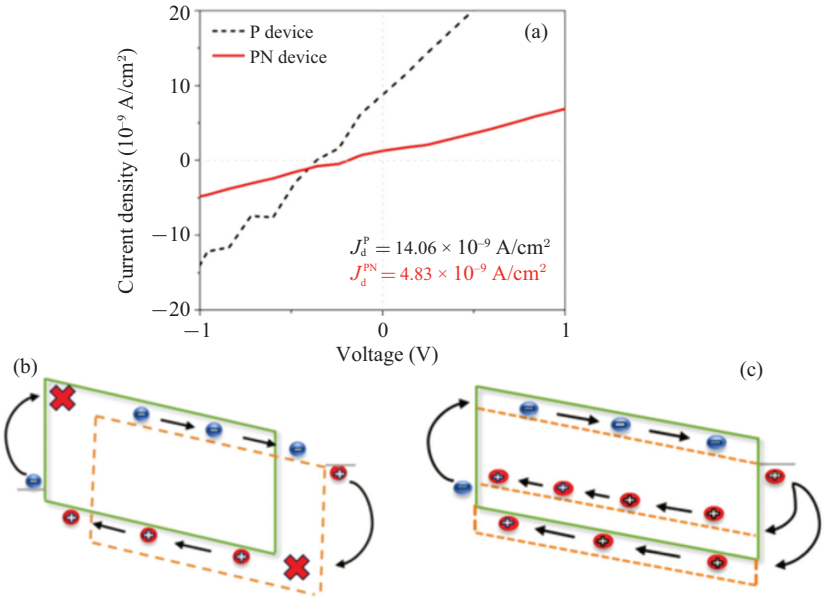


Fig. 3. The dark current density voltage characteristics for the P and PN structures. The dark current reduction mechanism of (b) vertical phase segregation, and (c) the presence of deep HOMO level.

3.3. Resistance and current against varying electric field analysis

To further study the basic characteristics of the devices under illumination and dark conditions, the current–electric field (*I*–*E*) curves and resistance–electric field (*R*–*E*) curves were plotted.[33] The electric field was calculated using the formula $E = V/d$, where V is the voltage while d represents the device's thickness. The thickness of the P device was found to be 150 nm, while the thickness of the PN device was 160 nm. The *I*–*E* curves for both devices are shown in Fig. 4(a).

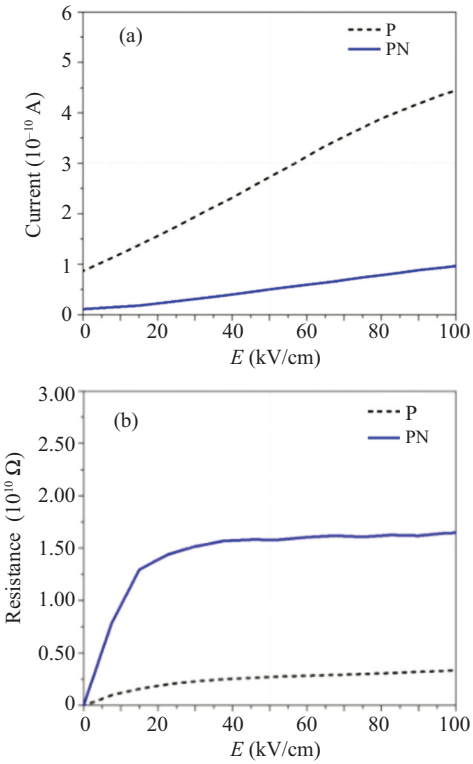


Fig. 4. (a) The current–electric field characteristics and the (b) resistance–electric field characteristics for the P and PN structures.

The electric field drives the charge carriers through the device leading to a current flow. If the strength of the electric field is sufficient to overcome the Φ_b at the photoactive:electrode interface, then the electrons and holes can tunnel through and become mobile charges leading to a more significant dark current. The values of dark currents for both P and PN devices at $E = 100$ kV/cm were found to be 4.47×10^{-10} A and 0.97×10^{-10} A, respectively. Thus, a decrease in dark current is observed due to the addition of OXCBA at $E =$ 100 kV/cm which further reaffirms less charge injection due to an increase in the charge injection barrier because of the deep HOMO level of OXCBA.

The resistance was calculated using the Ohmic relation ($R = V/I$), and the *R*–*E* curves were plotted as shown in Fig. 4(b). The resistance in the horizontal direction gradually increased for both devices, irrespective of the wavelength. However, the PN device showed an increasing resistance trend under dark conditions compared to the P device. In the case of dark conditions, the increase in resistance can be attributed to the reduction in the charge injection current from the electrode due to OXCBA.[34]

Specific detectivity or D^*_{shot} is a figure of merit used to evaluate the performance of a photodetector in terms of signal-to-noise ratio (S/N), detector area, and detection bandwidth. The formula to determine is given as[35–37]

$$D^*_{shot} = \frac{R}{\sqrt{2qJ_d}}, \tag{2}$$

where R represents responsivity, J_d represents dark current density, and q is the electric charge of an electron. The higher the is the better device performance. Another important parameter in evaluating the performance of the photodetector is the S/N ratio with respect to the dark current, where I_{light}/I_{dark} is at a certain applied voltage.[38,39] These values for both devices are tabulated in Table 1.

The S/N rvalue was increased in the PN device, confirming that the presence of OXCBA in the VOPcPhO host enhanced the photodetector's performance. The D^*_{shot} for all the lateral devices was obtained in the order of 10^{11} Jones (see Table 2), which is comparable with the values obtained for vertical structures in the previous literature.[40–42]

Table 1. The P and PN device's dark current and values.

Devices	J_d (nA/cm^2)	Responsivity (nA/W)	S/N	D^*_{shot} (10^{11} Jones)
P	14.06	254.0	0.722 (at −1 V)	1.197
PN	4.83	175.8	1.45 (at −1 V)	1.414

Table 2. Comparisons between vertical UV-OPDs based on small molecules and present work.

Devices	Voltage/bias	J_d (A/cm^2)	D^* (10^{11} Jones)	Ref.
ITO/TAPC:MoO_3/active layer/Bphen/Ag	at −3 V	1.11×10^{-9}	64.3	[41]
ITO/TPBi/MoO_3/C70/active layer/BCP/Al	at −6 V	2.2×10^{-2}	22	[40]
ITO/PEDOT:PSS/active layer/Bphen/Ag	at −1.5 V	4.82×10^{-7}	3.7	[42]
Al/VOPcPhO:OXCBA/Al (lateral configuration)	at −1 V	$4.83 \times 10_{-9}$	1.414	this work

4. Conclusion

This work's fabrication and characterization of a VOPcPhO-based UV organic photodetector provided valuable insights into the performance and design considerations. Furthermore, a VOPcPhO:OXCBA device mixed in a 1:1 molar ratio was also fabricated. The influence of OXCBA as an additive and its role in mitigating the dark current density was studied under a 45 mW/cm^2 UV light source. One notable achievement of this study is the reduction of dark current density in the VOPcPhO:OXCBA device, resulting in low values of 4.83 nA $\cdot$ cm^{-2} as compared to a stand-alone VOPcPhO of 14.06 nA $\cdot$ cm^{-2}.

Acknowledgment

The authors would like to acknowledge the financial support from the Ministry of Science, Technology and Innovation with Grant No. MOSTI004-2023SRF.

References

[1] Li Q, Guo Y and Liu Y 2019 *Chem. Mater.* **31** 6359
[2] Wang H, *et al.* 2017 *Adv. Mater.* **29**
[3] Li G X, Wang Y K, Huang L X and Sun W H 2022 *ACS Appl. Electron. Mater.* **4** 1485
[4] Bao C X, Yang J, Bai S, Xu W D, Yan Z B, Xu Q Y, Liu J M, Zhang W J and Gao F 2018 *J. Adv. Mater.* **30** 1803422
[5] Xie C, Lu X T, Tong X W, *et al.* 2019 *Adv. Funct. Mater.* **29** 1806006
[6] Biswas B and Saha B 2019 *Phys. Rev. Mater.* **3** 020301
[7] Dou L T, You J B, Hong Z R, *et al.* 2013 *Adv. Mater.* **25** 6642
[8] Baeg K J, Binda M, Natali D, *et al.* 2013 *Adv Mater.* **25** 4267
[9] Abdullah S M, Ahmad Z, Aziz F and Sulaiman K 2012 *Org. Electron.* **13** 2532
[10] Zafar Q, Ahmad Z, Sulaiman K, *et al.* 2014 *Sens. Act. A: Phys.* **206** 138
[11] Pan J, Deng W, Xu X Z, Jiang T H, Zhang X J and Jie J S 2019 *Chin. Phys. B* **28** 038102
[12] Pierre A, Deckman I, Lechêne P B and Arias A C 2015 *Adv. Mater.* **27** 6411
[13] Chow P C and Someya T 2020 *Adv. Mater.* **32** 1902045
[14] Esopi M R, Calcagno M and Yu Q 2017 *Adv. Mater. Technol.* **2** 1700025
[15] Agostinelli T, Campoy-Quiles M, Blakesley J C, Speller R, Bradley D D C and Nelson J 2008 *Appl. Phys. Lett.* **93** 203305
[16] Wang H Y, Xing S, Zheng T F, *et al.* 2018 *ACS Appl. Mater. Int.* **10** 3856
[17] Biele M, Benavides C M, Hürdler J, Tedde S F, Brabec C J and Schmidt O 2019 *Adv. Mater. Technol.* **4** 1800158
[18] Kim H U, Park O Y, Park J B and Hwang D H 2016 *J. Nanosci. Nanotechnol.* **16** 10465
[19] Kim K H, Kang H, Nam S Y, *et al.* 2011 *Chem. Mater.* **23** 5090
[20] Hisamuddin S N, *et al. Synthetic Metals* 2020 **268** 116506
[21] El-Nahass M M, Abd-El-Rahman K F, Al-Ghamdi A A and Asiri A M 2004 *Physica B* **344** 398
[22] Senthilarasu S, Sathyamoorthy R, Lalitha S, Subbarayan A and Natarajan K 2004 *Sol. Energy Mater. Sol. Cells* **82** 179
[23] El-Nahass M, Zeyada H M, Aziz M S and El-Ghamaz N A 2004 *Opt. Mater.* **27** 491
[24] Coulter J B and Birnie D P III 2018 *Phys. Status Solidi B* **255** 1700393
[25] Aziz F, Sulaiman K, Karimov K S, Muhammad M R, Sayyad M H and Majlis B Y 2012 *Mol. Crys. Liq. Crys.* **566** 22
[26] Dong H, *et al.* 2012 *Chemical Society Reviews* 2012 **41** 1754
[27] Murugesan V S, *et al.* 2015 *International Journal of Photoenergy* **2015**
[28] Simone G, *et al.* 2020 *Adv. Funct. Mater.* **30** 1904205
[29] Simone G, *et al.* 2020 *Adv. Opt. Mater.* **8** 1901568
[30] Md Sabri A A, Natashah F A, Hisamuddin S N, *et al.* 2022 *Photonics* **9** 947
[31] Hisamuddin S N, *et al.* 2020 *Synthetic Metals* **268** 116506
[32] Sharma N, *et al.* 2019 *Opt. Mater.* **95** 109273
[33] Kim T, *et al.* 2022 *ACS Appl. Electron. Mater.* **4** 130
[34] Ren H, *et al.* 2021 *Adv. Sci.* **8** 2002418
[35] Fang Y, Armin A, Meredith P and Huang J 2019 *Nat. Photon.* **13** 1
[36] Zhao X, Li X, Liu M, *et al.* 2024 *Acta Phys. Chim. Sin.* **40** 2311021 (in Chinese)
[37] Zhao X, Liu M, Wang J, *et al.* 2024 *ACS Appl. Mater. Int.* **16** 35400
[38] Liu M, Yao Q, Li S, *et al.* 2024 *Adv. Opt. Mater.* **12** 2303216
[39] Basir A, Alzahrani H, Sulaiman K, *et al.* 2021 *Physica B* 2021 **600** 412546
[40] Guo D, Yang D Z, Zhao J C, Vadim A and Ma D G 2020 *J. Mater. Chem. C* **8** 9024
[41] Lee C C, Biring J, Ren S J, *et al.* 2019 *Org. Electron.* **65** 150
[42] Wang X, Wang J Y, Zhao H M, Jin H and Yu J S 2019 *Mater. Lett.* **243** 81